ACS APPLIED MATERIALS & INTERFACES

Research Article

www.acsami.org

Direct Measurement of Surface Dissolution Rates in Potential Nuclear Waste Forms: The Example of Pyrochlore

Cornelius Fischer,*[,†,‡] Sarah Finkeldei,[§] Felix Brandt,[§] Dirk Bosbach,[§] and Andreas Luttge[†,‡]

[†]MARUM & FB5 Geowissenschaften, Universität Bremen, Klagenfurter Strasse, D-28359 Bremen, Germany

[‡]Earth Science Department, Rice University, 6100 Main Street, Houston, Texas 77005, United States

[§]Institute of Energy and Climate Research, Nuclear Waste Management and Reactor Safety (IEK-6), Forschungszentrum Jülich, D-52425 Jülich, Germany

ABSTRACT: The long-term stability of ceramic materials that are considered as potential nuclear waste forms is governed by heterogeneous surface reactivity. Thus, instead of a mean rate, the identification of one or more dominant contributors to the overall dissolution rate is the key to predict the stability of waste forms quantitatively. Direct surface measurements by vertical scanning interferometry (VSI) and their analysis via material flux maps and resulting dissolution rate spectra provide data about dominant rate contributors and their variability over time. Using pyrochlore ($Nd_2Zr_2O_7$) pellet dissolution under acidic conditions as an example, we demonstrate the identification and quantification of dissolution rate contributors, based on VSI data and rate spectrum analysis. Heterogeneous surface alteration of pyrochlore varies by a factor of about 5 and additional material loss by chemo-mechanical grain pull-out within the uppermost grain layer. We identified four different rate contributors that are responsible for the observed dissolution rate range of single grains. Our new concept offers the opportunity to increase our mechanistic understanding and to predict quantitatively the alteration of ceramic waste forms.

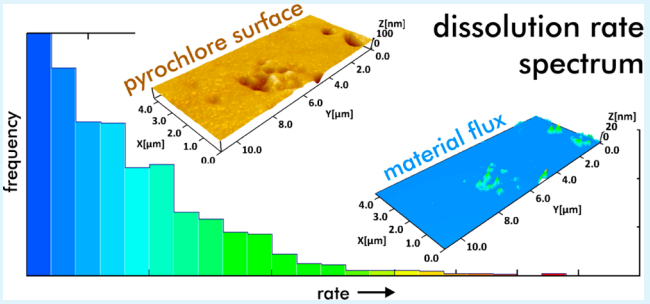

KEYWORDS: *nuclear waste management, dissolution rates, reactive surface portions, rate variability, rate spectra, pyrochlore, zirconates, vertical scanning interferometry*

1. INTRODUCTION

The evaluation of the stability of nuclear waste forms requires our ability to predict dissolution rates of fluid−solid reactions with high reliability for long time periods of many thousands of years. The reaction rates of natural and technical materials, determined under similar laboratory conditions show broad variations, often several orders of magnitude.[1−5] Even though these effects were already attributed to properties of the material under investigation, e.g., single crystals versus polycrystalline ceramics, so far no systematic understanding of the different contributors to the overall rate has been provided. Here, a new approach is required to study and quantify the evolution of surface rate heterogeneity in order to understand the mechanisms of rate variability for this specific application. Direct surface measurements offer the opportunity to detect and quantify diverse contributions to the overall reaction rate.[6−8] Such measurements provide information about the spatial heterogeneity of material loss during corrosion. Both statistical treatment as well as spatial and temporal analysis of surface rate data provide important insight into the stability of single contributors to the overall rate.[9] Such information are not available from the classical approach using a single rate constant and the calculation of a standard deviation. Moreover, resulting data of surface-sensitive rate analysis inform about the anisotropic evolution of porosity and permeability with critical consequences for potential functional failure of the material.

1.1. Nuclear Waste Forms and Pyrochlore as Potential Waste Form.

Ceramics are considered as alternative to well-established nuclear waste forms such as borosilicate glasses or to the direct disposal of spent nuclear fuel.[10,11] The main advantage of ceramics is their capability to serve as a tailor-made waste form for specific radionuclides, e.g., plutonium or special waste streams, e.g., the minor actinides (MA = Am, Cm, Np).[12] For many ceramic systems natural analogues have confirmed the suitability to immobilize for several million years.[12] Because of their inherent crystallinity, ceramics embed radionuclides on well-defined lattice positions within the particular crystal structure. Many ceramics exhibit a relatively high aqueous durability and tolerance against radiation which makes ceramics even more attractive as potential waste forms. Besides monazite, perovskite, and zirconolite, particular interest is dedicated to pyrochlores. Zirconate pyrochlores with the general chemical composition $A_2B_2O_7$ with B = Zr seem to be highly promising materials for the immobilization of plutonium and MA.[13] Zirconate pyrochlores have been investigated in

Received: May 17, 2015
Accepted: July 17, 2015
Published: July 17, 2015

DOI: 10.1021/acsami.5b04281
ACS Appl. Mater. Interfaces 2015, 7, 17857−17865

terms of their slow dissolution kinetics as a function of temperature and pH and with respect to the release of the A component.[14,15]

Many dissolution studies of potential nuclear waste forms in the literature have used macroscopic approaches.[16−18] Recently microscopic approaches were applied to gain a deeper understanding about the variability of the dissolution rates and the contribution of different dissolution mechanisms. Microscopic studies via SEM described the dissolution at grain boundaries of polycrystalline pyrochlore, CeO_2, and ThO_2 as well as $Ce_{1-x}Ln_xO_{2-x/2}$ ceramics.[19−21] These studies especially highlight the apparent preferential dissolution at grain boundaries whereas the retreat of the pellet surface is hardly accessible by SEM and the pellet surface itself seems to be rather unreactive from SEM observations. Information about material release via surface normal retreat and single grain dissolution are not yet available. This shortcoming was overcome in recent studies by assuming dimensions of surface features such as pores to have equal dimensions in horizontal and vertical dimensions.[21] Surface sensitive techniques with nanoscale resolution such as atomic forcae microscopy (AFM) and vertical scanning interferometry (VSI) allow to unravel dissolution mechanisms at the ceramic surface itself. So far, most dissolution studies using AFM have been performed for single-crystal samples.[22−25] Here, we investigate quantitatively the dissolution of polycrystalline material using VSI technique that provides a large-enough field-of-view. We present and analyze new experimental results obtained on a polycrystalline ceramic using pyrochlore as a case study for a potential nuclear waste form.

1.2. Analysis of Rate Contributors. Using a surface sensitive method with high spatial resolution and large field-of-view offers the opportunity to answer the following critical questions: Is the material flux during dissolution dominated by a largely homogeneous surface normal retreat or by local contributions, such as isolated single grain dissolution? Does the corrosion of polycrystalline material result in an evolution of multiple pore types with potential consequences on permeability during long-term dissolution? Answers to these questions are provided by the analysis of time series of surface maps that are used to calculate material flux maps in the spatial domain and rate spectra histograms in the frequency domain.[9]

In this study, we apply surface direct analysis using vertical scanning interferometry (VSI) to identify and quantify site-specific material release from the reacting surface.[8,26] Additionally, AFM surface data are used to provide information with higher lateral resolution. The resulting data sets inform about material flux from the reacting surface and are analyzed using the rate spectra approach.[9,27] The strength of this relatively new approach has been demonstrated already for polycrystalline material[27] and, consequently, first applications of the concept for such materials have been published.[28,29]

With this study, we demonstrate how the range of and the dominant contributors to the overall rate during dissolution of a polycrystalline potential waste form are quantified and systematically analyzed. For the first time, deconvolutions of complex rate spectra are calculated in order to analyze the number and amplitude of rate contributors. Thus, we expect conclusions from this study for the application of multiple rate contributors vs a single mean rate for the enhanced predictability of material release and the evolution of porosity and permeability in polycrystalline material.

Our strategy for this study is to identify and analyze material sections with contrasting reactivity. Rather than homogeneous surface-normal retreat, the dissolution of polycrystalline solids does result in heterogeneous surface material flux from certain sources such as (i) single grains with higher reactivity compared to other grains with lower reactivity, due to, for example, crystallographic orientation;[30] (ii) intergrown grain aggregates;[9] and (iii) chemo-mechanical release of material governed by a combination of material dissolution, weakening of the material structure, and subsequent mechanical grain pull-out.[28]

2. METHODS

2.1. Preparation of Pyrochlore Pellets. A wet chemical approach was applied to obtain pyrochlore powders. A detailed description of the pyrochlore powder precipitation can be found elsewhere.[13] Two pellets were fabricated from the pyrochlore powder with the same conditions. One was used for the characterization techniques whereas the second pellet was used for the dissolution study. The pyrochlore ceramic with a diameter of 10 mm was fabricated with an uniaxial hot press at 1550 °C and 3.9 kN after a precompaction of the powder via cold pressing at 50 kN. A resintering step at 1100 °C in air was applied to balance the oxygen deficit.

The final polishing was achieved with a diamond paste of 1 μm size. The pellet had a density of 99.5% theoretical density, which was measured via the Archimedes' principle. The pellet was characterized by powder X-ray diffraction to probe the pyrochlore crystal structure. Diffraction pattern were measured between 10−90 2θ with a D4 (θ−2θ geometry) from Bruker AXS GmbH. Figure 1 illustrates the microstructure of the polished pyrochlore ceramic pellet prior to and after the dissolution experiment. Initially, the pellet shows a highly dense microstructure and low porosity. Based on previous experiments[19,31] using the same $Nd_2Zr_2O_7$ ceramics, a chemical material contrast can be excluded and thus the contrast in the backscattered electron image is caused by the different crystallographic orientations of the grains. TEM analysis including EDX spot measurements were performed using samples prepared under identical conditions. No chemical zoning of grains and no enrichment of Nd or Zr at the grain boundaries or grain center has been observed.[32]

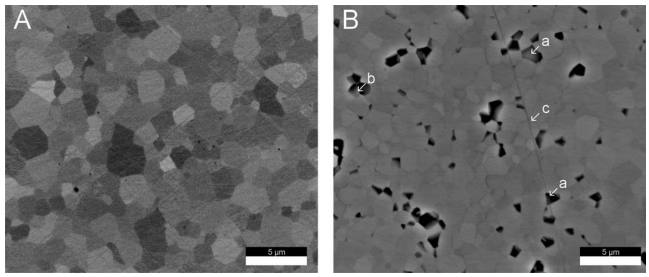

Figure 1. (A) Backscattered SEM image of the polished pristine pyrochlore pellet surface. BSE contrast illustrates variability of crystal orientation. Note the high density and low porosity of the pyrochlore ceramics. (B) SEM image of the reacted pyrochlore surface after 60 h reaction time. (a) Grain pull-out results in surface pores of size and shape of single pyrochlore grains having rounded pore walls according to triple-point geometries. In contrast, (b) flat pores show pore wall morphologies similar to etch pit shapes. Note that surface scratches (c) do not contribute significantly to any preferred dissolution.

The grain size differs approximately between one and four micrometers. Scratches on the surface are originated by the polishing procedure. Such scratches do not result in enhanced dissolution (Figure 1B, (c)). Most of the pores are located at grain boundaries or triple junctions whereas minor intragranular porosity is also visible. The pore size is in the submicrometer scale. Distinct grain boundaries are visible in the backscattered SEM image. Prior to the dissolution experiment the pellet was treated with acid in order to remove possible

DOI: 10.1021/acsami.5b04281
ACS Appl. Mater. Interfaces 2015, 7, 17857−17865

surface contaminations due to preparation and polishing. This sample is referred to as pristine sample in the present study. The pristine pellet surface shows a curvature of about 20−40 nm in height per unit length of 1 mm.

2.2. Experimental Section. A batch dissolution experiment was performed in a Teflon reaction vessel (volume = 50 mL). The applied experimental conditions (4 M HCl, 90 °C) were chosen on the basis of previous static and dynamic dissolution experiments on $Nd_2Zr_2O_7$.[19,31] A constant temperature was provided using a drying oven. At the conditions of the experiments, pyrochlore is metastable and therefore dissolution can be assumed to be at far from equilibrium conditions. A detailed discussion about the thermodynamics of pyrochlore and its dissolution can be found elsewhere.[19] To analyze the pellet surface using VSI technique, we took the pellet out of the dissolution medium, rinsed it with distilled water, and dried it. Dissolution experiments have been performed over a period of 420 h in total. The reacting surface has been analyzed after 24, 40, 60, 81, 250, and 420 h, respectively. To avoid the possible precipitation of secondary phases, we always replaced the dissolution medium after each characterization step by VSI. The fresh dissolution medium was every time preheated to 90 °C before the sample was placed into the Teflon reaction vessel.

2.3. Sample Height Reference. Prior to dissolution experiments, the pellet sample surface was partially covered with a PTFE foil. The uncovered sample surface was then masked with a gold layer using physical vapor deposition (PVD) technique. The inert Au layer served as a height reference during the dissolution experiment. After removal of the Teflon foil the thickness of the gold layer was analyzed using VSI technique to be 640 ± 20 nm (Figure 2A, B).

Since the sample shows a curvature and relief of 40 nm in height per unit length of 1 mm, the precision of height difference calculations is limited to this uncertainty. An increase of the height difference between layer surface and material surface can be used to quantify surface normal retreat of the altered material surface. Height difference measurements between the gold mask surface and the reacted pyrochlore surface have been performed using a histogram analysis of data sets with a size of 750 μm × 750 μm. A section of such a topography data set is shown in Figure 2A. Half of each analyzed field contains data points of the surface mask. The height distance of resulting histogram peaks, i.e., gold surface height and uncovered sample surface height is used to quantify a surface normal retreat of the sample surface with respect to the inert mask surface.

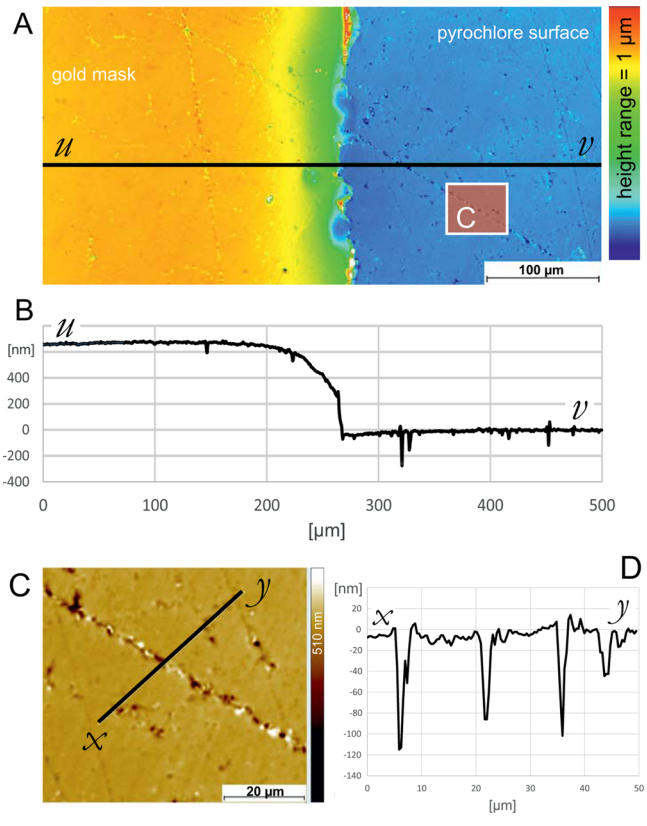

Figure 2. (A) Map and (B) profile of a gold mask on a pyrochlore pellet sample. Thickness of the gold layer is 640 ± 20 nm. After an initial dissolution period, the pyrochlore surface shows roughness in the submicrometer range. (C) A map prior to dissolution shows trails of pores with depth of about 100 nm, see (D) profile.

2.4. Analysis of Surface Topography. Surface topography evolution has been quantitatively analyzed using vertical scanning interferometry (VSI) technique. Surface topography changes were measured at each time step using a Zemetrics ZeMapper (Tucson AZ) VSI equipped with 2048 × 2048 pixel CCD camera and four Mirau and a Michelson objectives. VSI measures the surface topography of a sample at high vertical (~1 nm, white light mode) resolution. Using a 100× Mirau objective (NA = 0.8), the calculated lateral resolution in the same optical plane is 0.42 μm, while the lateral resolution of a three-dimensional object is clearly higher and in the range of about 100−150 nm using the ZeMapper instrument.[33] The largest field-of-view (FOV) that is obtained using this instrument and a 5× Michelson interferometer objective is 3 mm × 3 mm. The highest lateral resolution is obtained using a 100× Mirau objective with 1.6× magnification lens. We applied this setup for material flux map analysis (see below), using a FOV of 95 μm × 95 μm.

To quantify a reaction rate, the change in topography is mapped by measuring the surface before and after reaction. The change in height at a fixed point on the surface over a time interval results from either retreat via dissolution or advance by growth of the surface. The reaction rate at each point of the surface is given by the velocity of height changes (dh/dt). The application of VSI to the measurement of reaction rates and characterization of surface topography is well-documented.[8,9] We applied identical (x,y,z) coordinates using landmarks of the masked area of the sample and constant tip/tilt angle data of the sample stage in order to get a sequence of leveled surface map data that are applicable for material flux calculations. Further details regarding VSI instruments and associated physical principles are available elsewhere.[27]

Initially, large sections of the sample surface show a rough surface with a variability in height of 10 nm (Figure 2C, D). These information are accessible by VSI which points out the complementary information that can be gained by this method in comparison to the SEM analysis (Figure 1) and macroscopic approaches. Additionally, deeper surface scratches and pores exist owing to the polishing procedure that has been applied. Such surface deviations are in a height range of 100 nm (Figure 2C, D).

Additional surface measurements with higher lateral resolution were performed using atomic force microscopy (AFM). We utilized a Dimension FastScan system (Bruker) with an Icon Scanner and TESPA-V2 cantilevers in tapping mode.

During the entire dissolution experiment, no formation of a leached layer was observed, even though a preferential release of Nd compared to Zr is well-known for the acidic pH range.[14,15,19,31]

2.5. Statistical Analysis of Surface Topography Data. A time series of surface data contains two important pieces of information. First, surface difference maps can be used to quantify and visualize the material flux distribution that contributes to the overall surface reaction rate. Histogram analysis of flux maps result in reaction rate spectra that provide information about frequency of rate contributors to the overall rate.[9,27] Second, surface data analysis provides quantitative information about evolution of topography via surface roughness parameters. Heterogeneous contribution to overall surface roughness, i.e., the existence of surface building blocks of specific size and distribution can be analyzed quantitatively by using converged roughness parameters.[9,34] Accordingly, this approach has been applied before to calculate roughness parameters[35] such as root-mean-square (RMS) roughness, Sq:

DOI: 10.1021/acsami.5b04281
ACS Appl. Mater. Interfaces 2015, 7, 17857−17865

$$Sq = \sqrt{\frac{1}{MN}\sum_{k=0}^{M-1}\sum_{l=0}^{N-1}[z(x_k, y_l)]^2}$$

We calculated the Sq parameter data for FOV sizes varying from 10 μm up to 300 μm using 52 data sets collected by VSI technique.

To avoid any impact of surface scratches on the analysis of surface roughness, porosity, and surface rates, we selected surface map sections free of scratches for the quantitative analysis. Nevertheless, Figure 1B (c) illustrates the negligible impact of surface scratches to overall surface rates.

3. RESULTS AND DISCUSSION

3.1. Surface-Normal Retreat. The initial pyrochlore pellet surface shows a curvature and relief of at maximum 40 nm in height per unit length of 1 mm, cf. methods section. This height variability of the surface is passed on to the gold reference surface, resulting in an uncertainty of the reference height within 20−40 nm. With respect to this height variability, no surface normal retreat smaller than 40 nm can be detected and quantified. Table 1 shows data of height difference measurements between the gold mask surface and the reacted pyrochlore. Height difference data indicate no measurable surface normal retreat for reaction periods of up to 250 h. Height data after a reaction time of 420 h indicate a surface normal retreat of 40 ± 20 nm. The absence or very minor surface normal retreat offers however the opportunity to study the initial evolution of flat pores with depths in the range of single to tens of nanometers and related rough surface topography with high precision and in greater detail.

Table 1. Mean Height Difference Data and Standard Deviation between an Inert Gold Mask Surface and the Reacted Pyrochlore Pellet Sample Surface

reaction time (h)	height (nm)
24	640 ± 20
40	640 ± 20
60	640 ± 20
81	630 ± 20
250	650 ± 20
420	680 ± 20

3.2. Evolution of Pores. VSI measurements provide surface data and, thus, inform about the evolution of pore size and depth. Figure 3 shows a comparison of the topography of the pyrochlore surface after reaction periods of 40 and 420 h, respectively. The overall height range of 1 μm is identical for the resulting rough surfaces of both reaction steps. Figure 3 informs about the existence of two major pore types. Large pores have a lateral extension of several micrometers and a depth close to 1 μm. Such pores exist already after the short reaction period of 40 h. The comparison of these data sets underscores the evolution of flat pores: After 40 h of reaction (Figure 3A, inset), the overall topography is still smooth and only a few flat pores (depth <20 nm) have been detected. After 420 h of reaction, however, the frequency of flat pores is remarkably higher and some of them have a depth of more than 100 nm. The lateral size of all flat pores is constant and similar to the diameter of single pyrochlore grains with a size of about 1 μm, cf. Figure 1. Thus, the major material flux due to dissolution results in the vertical growth of flat pores that are bound to single-grain corrosion. This reflects contrast in surface retreat of single-crystal faces.

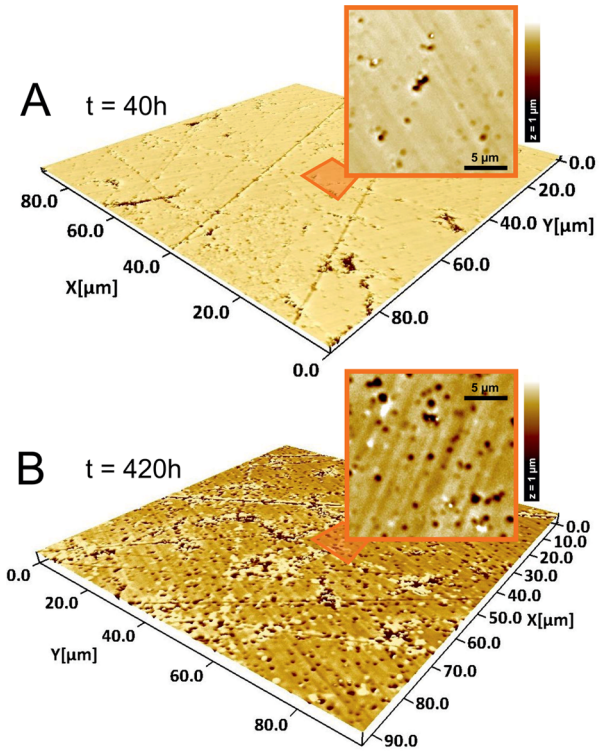

Figure 3. Pyrochlore surface topography after dissolution periods of (A) 40 and (B) 420 h. Note the identical height range of 1 μm and the strong increase in number of flat and small pores from A to B. Large and deep pores (dark sections in A) have a similar depth like such pores in section B of about 1 μm.

Figure 4 visualizes and quantifies the heterogeneous surface topography of pyrochlore resulting from a reaction period of 420 h. In general, the pellet surface consists of several building blocks, i.e., plateaus, flat pores, and deep pores. In contrast to most SEM pictures, the VSI data allow for a quantification of both, lateral and vertical pore dimension. The lateral dimension of the plateaus and deep pores is often larger than a single pyrochlore grain diameter (1−4 μm). The lateral dimension of flat pores is usually identical to the grain size of pyrochlore. However, the vertical dimension of the surface building blocks is more diverse. Figure 4A illustrates the variability of the depth of flat pores (types 1−3) that range from 60 to 115 nm. We identified four classes of pore depths. This is a new result compared to the previously assumed almost constant pore depth.[21] Further investigation is needed to identify whether specific crystal orientation and/or other factors are responsible for the observed types of pore depths.

Depth variability of deep pores (type 4) is not as diverse; most of them have a depth of about 1 μm what is similar to the mean crystal size.

Plateau-shaped building blocks (pl) are the uppermost surface sections. According to height data of an inert sample section (Table 1) and the quantification of surface normal retreat, these surface portions may represent remnants of the unreacted surface. They occur only after the long-term reaction of 420 h. Their mean height above the lowered sample surface is about 40 nm. The smallest lateral dimension of the plateau shaped building blocks is about 1−2 μm. This is similar to the size of single grains of pyrochlore in this sample.

An AFM surface map (Figure 5) shows the typical shape and size of such a plateau building block with higher lateral

DOI: 10.1021/acsami.5b04281
ACS Appl. Mater. Interfaces 2015, 7, 17857−17865

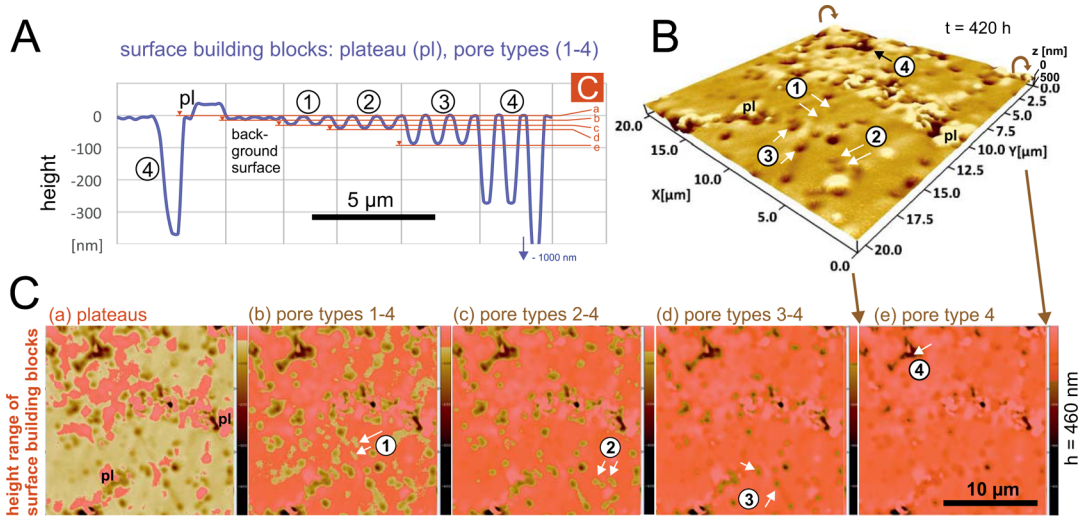

Figure 4. Surface topography of a pyrochlore pellet sample after a reaction time of 420 h. (A) Exemplified height profile of important surface building blocks; pl, (mostly) unreactive plateaus, height = 40 nm; 1, flat pores, mean depth = 60 nm; 2, flat pores, mean depth = 70 nm; 3, flat pores, mean depth = 115 nm; 4, deep pores, depth 300−1000 nm. (B) VSI data set visualizes the spatial occurrence of building blocks explained in A. (C) Surface map sequence (a−e) shows frequency and distribution of surface building blocks (pl, 1−4) via height discrimination (red, cf. A)), color-coded height range = 460 nm.

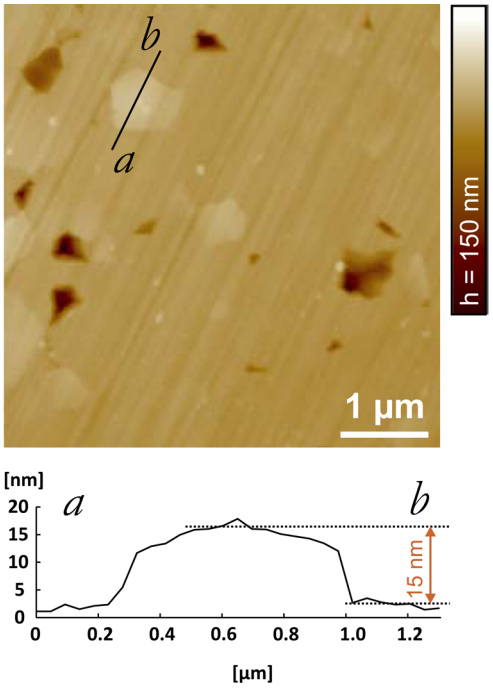

Figure 5. AFM map and profile of a polycrystalline pyrochlore surface section after a reaction period of 420 h. The data visualize the contrast in surface retreat of single pyrochlore grains. Light-colored sections in the map indicate crystal faces with low retreat rates and, thus, low surface reactivity. Resulting maximum height difference is about 15 nm, see profile (lower part).

resolution. The AFM data showing positive surface features support the interpretation that surface plateaus consist of single pyrochlore grains because of their characteristic shape. Furthermore, the data indicate the existence of a fraction of almost inert grains within this specific sample configuration. Until now there are no information available that would explain such remarkable low reactivity of single pyrochlore grains. Nevertheless, the existence of contrasting reactivity of crystal faces has been described in the literature, for example, for different faces of fluorite crystals.[30] Thus, the analysis of crystal orientation using EBSD technique and correlation of such data with high-resolution surface flux maps would be a helpful approach in future studies to identify potential sources of reactivity contrasts.

Figure 4B, C visualizes the spatial occurrence of surface building blocks. The plateau-shaped sections form often linear structures with an overall extension of more than 10 μm. The deep pores are either isolated small pores (single-grain size) or complex laterally bigger structures. Flat pore types 1−3 are mostly isolated surface building blocks and do not show any anisotropy in terms of their spatial distribution.

3.3. Surface Roughness. Using RMS roughness parameter *Sq*, surface roughness has been analyzed in order to trace the evolution of vertical pore dimensions (Figure 6). The concept of converged surface roughness analysis has been applied to

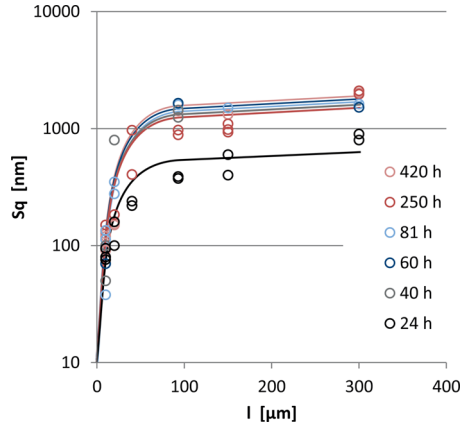

Figure 6. RMS roughness *Sq* as a function of field-of-view (FOV) size *l* for reaction steps at *t* = 24 to 420 h. Small FOV sections below *l* = 50 μm are associated with *Sq* < 500 nm. Large FOVs show convergence of *Sq* at about 1−2 μm owing to depth of grain pull-out pores within the uppermost grain layer for reaction periods >24 h. Error of *Sq* is within symbol size.

DOI: 10.1021/acsami.5b04281
ACS Appl. Mater. Interfaces 2015, 7, 17857−17865

provide information about roughness variability as a function of length scale.[34] This approach is mandatory for surfaces that do not show topographic self-similarity.[9] Topography alterations of materials that do not have constant and isotropic reactivity must not be analyzed using an approach of a simple fractal dimension or any roughness parameter without testing the scale dependency.

The measured plateau of converged RMS roughness *Sq* for FOV sizes $l > 100$ μm (Figure 6) underscores the narrow range of deep pore depths (type 4). The low *Sq* value for the initial prereacted surface (24 h) is caused by the limited number of such pores prior to longer reaction periods. The depth of deep pores is of similar size for all reaction periods longer than 24 h and is within the range of a single crystal diameter. This leads to the interpretation that the deep pores are caused by grain pull-out of single grains. This mechanism is described in the literature as chemo-mechanical corrosion of polycrystalline material.[28] Initial chemical corrosion at grain boundaries results in widened grain boundaries. Ultimately, it leads to mechanical disintegration and release of grains. Remarkably, for all reaction periods from $t = 40$ up to 420 h the maximum RMS roughness is similar (1−2 μm), indicating that the deep pores associated with chemo-mechanical corrosion are not able to grow to larger depth in our experiment. Thus, dissolution at grain boundaries is limited to the uppermost grain layer and the resulting chemo-mechanical corrosion is not able to cause larger pores during the analyzed reaction periods. An additional important information is that chemo-mechanical corrosion starts already during the initial corrosion periods (Figure 6, plateau for surface data from 40 h experiment). Both findings, the limited pore depth and the early occurrence of grain pull-out have important consequences for porosity and permeability evolution of pyrochlore ceramics during ongoing corrosion.

The occurrence of small *Sq* values for FOV sections $l < 50$ μm indicates the existence of surface sections of such lateral dimension that are not affected by the occurrence of grain pull-out pores. The broad roughness range (20−150 nm) reflects the occurrence of diverse flat pore types (1−3, Figure 4). Because roughness calculations lead to a sum parameter in terms of height distribution, the roughness data do not provide stable information about pore evolution during the experimental periods. Instead, the roughness range for FOV length below 50 μm shows a broad scatter, illustrating the contrast in surface reactivity that has been discussed above, see Figures 4 and 5.

3.4. Surface Reactivity. Figure 7 shows the increase in depth of flat pores during the dissolution experiment. Using a histogram analysis and associated depth discrimination (see Figure 4C), the increase in depth of three pore types was analyzed quantitatively. The existence of three flat pore types with fast (type 3) vs slow (type 1) dissolution kinetics underscores the existence of at least three major contributors to the overall dissolution rate. Depth of flat pore types 1 and 2 are analyzed for long reaction periods only. The reason for that are very small increments in depth of such pores that are similar to background topography fluctuations of a few nanometers only. In such cases, the signal-noise ratio is too low for a reliable quantification (sections with dashed line in Figure 7).

The results about contrasting pore depth evolution (Figure 7) have consequences for reaction rate quantifications. The data reveal that a mean rate value does not provide any mechanistic explanation nor quantitative predictive power in terms of polycrystalline pyrochlore dissolution. A simple mean

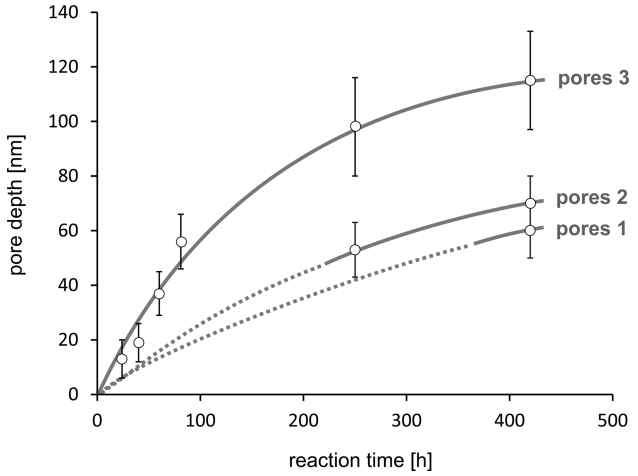

Figure 7. Depth evolution of three populations of flat pores over reaction time. The evolution of a second (flat pores 2, cf. Figure 4) and third (flat pores 1) population of flat pores was detected after a reaction period of 250 and 420 h, only. Lines serve as a guide to eye to visualize the pore depth evolution.

rate is not able to explain the formation of different types of pores during ongoing corrosion. Instead, the application of the rate spectrum approach provides explanation about the formation and evolution of multiple pore types.

The deconvolution of a measured rate spectrum results in specific modes. We define a rate contributor as a specific mode of the rate spectrum. Inversely, the superimposition of all rate contributors results in the complete rate spectrum. Rate contributions were quantitatively analyzed using the rate spectra concept.[9,27] As a prerequisite, a topography difference map was calculated using two VSI data sets of sample surface topography at reaction periods t_x and t_{x+1}. Figure 8 visualizes

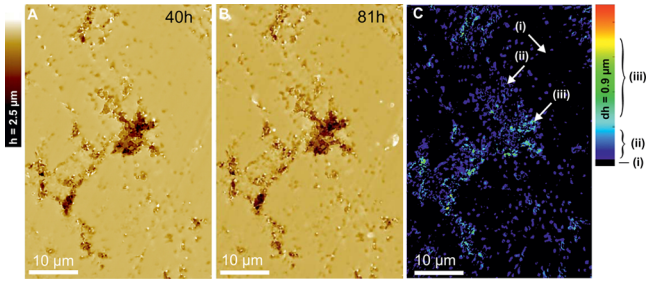

Figure 8. Topography data after (A) 40 and (B) 81 h dissolution periods. (C) Material flux map illustrates locally heterogeneous surface retreat during a reaction period of 41 h. Inert sections are indicated by black color (i). Two major populations of surface corrosion (mainly dark blue (ii, pore types 1−3, Figure 4) vs green/yellow color (iii, pore type 4, Figure 4)) have been identified.

the sample surfaces at reaction time $t = 40$ h (Figure 8A) and $t = 81$ h (B). The difference map (C) shows the corresponding material flux. During this reaction step, no measurable surface normal retreat exists. Consequently, the black background color represents no material flux. In fact, two general types of material flux were identified. Both, the dark and light-blue colors in Figure 8C illustrate moderate dissolution at surface spots having diameters of about one micrometer. This size represents either single grains/crystals of pyrochlore grains or grain aggregates including grain boundaries. Several green and yellow-colored spots of the flux map represent local surface

DOI: 10.1021/acsami.5b04281
ACS Appl. Mater. Interfaces 2015, 7, 17857−17865

retreat of more than 300 nm and up to one micrometer. Further, the material flux map shows the heterogeneous distribution of local material release. Remarkably large inert sections without any material flux do exist. Their size is up to about ten micrometers in diameter (large black sections, Figure 8C). The size of such inert sections comprises aggregates of multiple pyrochlore crystals. The reason for the existence of such large inert sections is not yet clear and requires further investigation by, for example, EBSD analysis of crystal orientation. A potential explanation is the occurrence of clusters of crystal aggregates having almost identical orientation and thus identical (low) surface reactivity.

In summary, polycrystalline pyrochlore shows heterogeneous dissolution behavior. A mean rate is thus not suitable to explain the dissolution of this material. Instead of a Gaussian distribution, multiple superimposed rate modes describe the dissolution of more or less reactive grains that form the ceramic sample surface. The material flux map (Figure 8C) was analyzed using the rate spectrum approach. The frequency analysis of the flux map contributors leads to a histogram with a shoulder toward higher material fluxes (Figure 9A). The

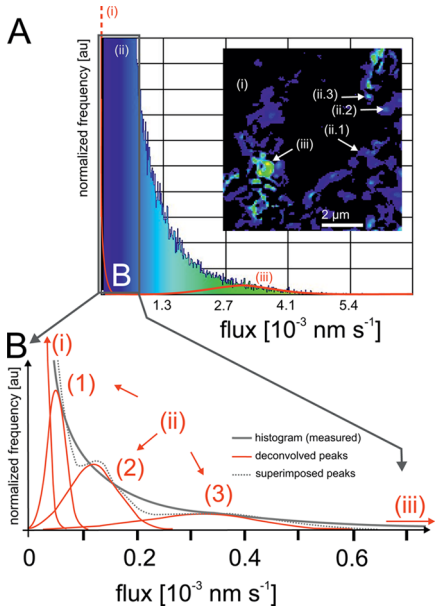

Figure 9. (A) Material flux spectrum for a reaction period of 41 h, frequency analysis of data from Figure 7C, using the same color code. Inset exemplifies corresponding material flux map. Peak (i) at zero position (= no surface-normal retreat) is clipped. (B) Visualization of deconvolution of the spectrum: (i) no flux = 0 nm; (ii.1) 8 ± 2 nm; (ii.2) 18 ± 4 nm; (ii.3) 50 ± 10 nm. Fourth peak at 500 ± 60 nm is shown in (A).

maximum of the histogram distribution is at about 0 nm. It represents surface sections without any measurable surface-normal retreat or material flux. Further deconvolution of the histogram shoulder (Figure 9A) identified additional rate contributors. In this specific case, four significant contributors (ii.1−3 and iii; Table 2) of the overall flux distribution (Figure 9B) were identified. Flux contributors ii.1−3 represent three different dissolution rates. Their localized spatial occurrence (Figure 8C) suggests mechanisms of either pyrochlore single grain dissolution or spatially limited dissolution at grain boundaries and triple points. Additionally, a remarkably fast rate contribution occurs (Figure 9A, B (iii), Table 2:

Table 2. Pyrochlore Dissolution Rate Contributors, According to Deconvolution of Rate Spectrum (see Figure 8)[a]

no. (Figure 9B)	rate spectrum contributor (nm)	rate (g m^{-2} day^{-1})	remarks
i	0 ± 2	0 ± 1.0 × 10^{-5}	no measurable surface normal retreat
ii.1	8 ± 2	4.0 × 10^{-5} ± 1.0 × 10^{-5}	dissolution, flat pores type 1 (Figure 7)
ii.2	18 ± 4	8.9 × 10^{-5} ± 2.0 × 10^{-5}	dissolution, flat pores type 2
ii.3	50 ± 10	2.5 × 10^{-4} ± 0.5 × 10^{-4}	dissolution, flat pores type 3
iii	500 ± 60	2.5 × 10^{-3} ± 0.3 × 10^{-3}	grain pull-out, deep pores type 4

[a]Reaction period of 41 h (81 h − 40 h). M = 582.9238 g/mol; V_m = 9.2611 × 10^{-3} m^3/mol.

contributor # (iii). This contribution is however not a true dissolution rate, it does not represent complete dissolution of material. This rate explains rather erosion or pull-out of undissolved or partly dissolved pyrochlore grains. This interpretation is based on the height differences that are associated with the respective sites in the flux map (Figure 8) and previous observations based on SEM pictures.[19]

The combination of both dissolution and grain pull-out contributions to the overall material flux during corrosion has been described in the literature.[28] Further literature results of kinetic Monte Carlo simulation calculations explained mechanistically how high kink-site densities on grain surfaces enhance the local material flux[26] that ultimately leads to grain pull-out.

In the present study, the identification of single rate contributors provides new opportunities for the quantification of reaction rates in polycrystalline materials. The deconvolution of the rate spectrum extracts quantitative data that allowed for the identification and comparison of three different contributors (Figure 9). Table 2 shows the corresponding data that originate from the three processes (i) surface-normal retreat, (ii) pore formation, and (iii) grain pull-out. The rates ii.1−3 correspond to the formation of pore types 1−3 (Figure 7).

As expected, the rate contributions (ii) of the rate spectrum are in reasonable good agreement with literature data of overall dissolution rates of pyrochlore.[19] However, the new data inform about three different flux contributors (i−iii). Such specific information is not available from the literature data. In fact, normalization of literature data based on observed porosity evolution without quantitative knowledge about contributor (iii)/grain pull-out would lead to incorrect estimations of dissolution rates by 1−2 orders of magnitude and, thus, wrong predictions about material fate.

First examples in the literature applied the rate spectra approach[27] to describe the heterogeneity of dissolution of fine-grained limestone (micrite).[27−29] Now, we provide the first deconvolution of a spectrum and the resulting quantitative comparison of the different rate contributors. In this example, they span a rate range of about 2 orders of magnitude (Table 2). These data provide two important new aspects. First, they inform about the number of contributors to the overall dissolution rate. As already discussed, we identified three contributors that dominate the dissolution. Thus, three different mechanisms govern the dissolution of polycrystalline

DOI: 10.1021/acsami.5b04281
ACS Appl. Mater. Interfaces 2015, 7, 17857−17865

pyrochlore. Surface-normal retreat is a consequence of the three above-mentioned mechanisms. The superimposition of growing etch pit mophologies leads ultimately to surface lowering. In our example that has grain surfaces with large contrasts in surface reactivity, no complete surface-normal retreat was observed (Figure 5). The minor impact of surface-normal retreat is quantified by the associated rate contributor (i) of the deconvolved spectrum. In general, this underscores that the deconvolution of rate spectra provides the complete information about different dissolution mechanisms and their interaction. As an example, any faster movement of etch pit stepwaves[36] and their superimposition resulting in a faster surface-normal retreat would then be quantified by the specific rate contributors (i) and (ii) in the spectrum. Another great potential of the analysis of rate contributors is their predictive power in terms of porosity evolution. We suggest time-resolved analysis and evaluation of rate contributors in future experiments. Such an analysis informs about the temporal stability and spatial occurrence of one or more rate contributors. These information are critical for the evaluation and estimation of pore space evolution. Because the spatial distribution of rate contributors is not homogeneous (Figure 9A, inset), sections of the material volume do inherit reactivity contrasts. The size of such sections comprises multiple grains of the material. The existence of such sections does result in a pattern formation that impacts the distribution of new large pores. We predict that rate spectra contributors identify and quantify such pattern, similar to the identification of the specific rate contribution by surface-normal retreat. In-turn, knowledge about the occurrence and size of such pattern can be applied directly to the analysis of parameters that impact the fabrication of pyrochlore ceramics. Ultimately, this strategy offers the potential to vary material properties at will. Beside this, the data about temporal stability of such rate contributors would provide valuable insight into the formation of pathways of higher permeability. We suggest to apply this approach to the analysis of data collected using techniques such as X-ray tomography in the μm range[37] or electron tomography in the nm range.[38] The combination of such rate spectra data that cover the critical observational range of the length scale will provide a thorough picture of permeability evolution. Such combined information are applicable for reactive transport calculations. Ultimately, we predict an application of the presented approach that provides the connection between rate spectra analysis and reactive transport modeling calculations.

4. SUMMARY AND CONCLUSIONS

Polycrystalline material such as pyrochlore ceramic dissolves heterogeneously. The application of surface sensitive methods such as VSI provides key information to map the material flux from the surface and provides data to analyze statistically the contributors to the rate spectrum. The deconvolution of a given/measured rate spectrum results in specific modes. We define a rate contributor as a specific mode of the rate spectrum.

In detail, we summarize and conclude:

The applicability of potential nuclear waste forms is critically controlled by our ability to predict quantitatively their reactivity. The dissolution kinetics of polycrystalline materials such as pyrochlore is represented by a complex rate spectrum, i.e., by multiple rate contributors. The new information about multiple rate contributors are a prerequisite for the mechanistic understanding of polycrystalline pyrochlore dissolution. A combination of experimental approaches and simulation calculations (kinetic Monte Carlo techniques) will be the next step to analyze the impact of single rate contributors on the overall reaction rate of polycrystalline material.

Although we observed dissolution of single grains that is governed by multiple reaction velocities, homogeneous surface-normal retreat is of limited importance, during the dissolution of polycrystalline pyrochlore. It thus follows that dissolution of polycrystalline material is quantified by multiple contributors and cannot be treated like a single crystal surface.

Surface sensitive methods such as vertical scanning interferometry with a large field-of-view allow for the identification of heterogeneous surface reactivity caused by multiple reaction mechanisms. The analysis of large field-of-view rate maps provides information about reactivity contrasts from the nanometer scale up to the millimeter scale.

Release of pyrochlore material is not limited to only dissolution reactions. Additionally, mechanical grain removal, so-called pull-out of individual grains occurs during to the dissolution process. This results in a chemo-mechanical erosion. If the pull-out process becomes a significant factor, then the overall removal rate is not a dissolution rate sensu strictu and does not compare to single-crystal dissolution rates. In any case, our method allows for a clear quantitative distinction between such dissolution and erosion rates.

AUTHOR INFORMATION

Corresponding Author

*E-mail: cornelius.fischer@uni-bremen.de.

Notes

The authors declare no competing financial interest.

ACKNOWLEDGMENTS

We thank the MARUM (Univ. Bremen) for ongoing support. We gratefully acknowledge support from the DFG (Grants Fi 1212-7 and INST 144/378-1 FUGG). S.F. thanks Dr. Andrey Bukaemskiy for assisting in pellet preparation. We thank AE E.R. Fisher and three anonymous reviewers for very helpful comments.

REFERENCES

(1) Casey, W. H.; Banfield, J. F.; Westrich, H. R.; McLaughlin, L. What do Dissolution Experiments tell us about Natural Weathering. *Chem. Geol.* **1993**, *105* (1−3), 1−15.

(2) Swoboda-Colberg, N. G.; Drever, J. I. Mineral Dissolution Rates in Plot-Scale Field and Laboratory Experiments. *Chem. Geol.* **1993**, *105* (1−3), 51−69.

(3) Becker, U.; Hochella, M. F.; Apra, E. The Electronic Structure of Hematite {001} Surfaces: Applications to the Interpretation of STM Images and heterogeneous Surface Reactions. *Am. Mineral.* **1996**, *81* (11−12), 1301−1314.

(4) Arvidson, R. S.; Ertan, I. E.; Amonette, J. E.; Luttge, A. Variation in Calcite Dissolution Rates: a Fundamental Problem? *Geochim. Cosmochim. Acta* **2003**, *67* (9), 1623−1634.

(5) Daval, D.; Hellmann, R.; Saldi, G. D.; Wirth, R.; Knauss, K. G. Linking nm-scale Measurements of the Anisotropy of Silicate Surface Reactivity to Macroscopic Dissolution Rate Laws: New Insights Based on Diopside. *Geochim. Cosmochim. Acta* **2013**, *107*, 121−134.

(6) Dove, P. M.; Platt, F. M. Compatible real-time Rates of Mineral Dissolution by Atomic Force Microscopy (AFM). *Chem. Geol.* **1996**, *127* (4), 331−338.

(7) Bosbach, D.; Hochella, M. F. Gypsum Growth in the Presence of Growth Inhibitors: A Scanning Force Microscopy Study. *Chem. Geol.* **1996**, *132* (1−4), 227−236.

DOI: 10.1021/acsami.5b04281
ACS Appl. Mater. Interfaces 2015, 7, 17857−17865

(8) Luttge, A.; Bolton, E. W.; Lasaga, A. C. An Interferometric Study of the Dissolution Kinetics of Anorthite: The Role of Reactive Surface Area. *Am. J. Sci.* **1999**, *299* (7−9), 652−678.
(9) Fischer, C.; Kurganskaya, I.; Schäfer, T.; Lüttge, A. Variability of Crystal Surface Reactivity: What do we know? (Review Article). *Appl. Geochem.* **2014**, *43*, 132−157.
(10) Donald, I. W.; Metcalfe, B. L.; Taylor, R. N. J. The Immobilization of High Level Radioactive Wastes using Ceramics and Glasses. *J. Mater. Sci.* **1997**, *32* (22), 5851−5887.
(11) Johnson, L.; Shoesmith, D. In *Radioactive Waste Forms for the Future*; Lutze, W., Ewing, R. C., Eds.; North-Holland: New York, 1988; Chapter 11, pp 635−698.
(12) Lumpkin, G. R. Ceramic Waste Forms for Actinides. *Elements* **2006**, *2* (6), 365−372.
(13) Ewing, R. C.; Weber, W. J.; Lian, J. Nuclear Waste Disposal—Pyrochlore (A2B2O7): Nuclear Waste Form for the Immobilization of Plutonium and "Minor" Actinides. *J. Appl. Phys.* **2004**, *95* (11), 5949−5971.
(14) Hayakawa, I.; Kamizono, H. Durability of an La2Zr2O7 Waste Form in Water. *J. Mater. Sci.* **1993**, *28* (2), 513−517.
(15) Hayakawa, I.; Kamizono, H. Durability of an $La_2Zr_2O_7$ Waste Form Containing Various Amounts of Simulated HLW Elements. *J. Nucl. Mater.* **1993**, *202* (1−2), 163−168.
(16) Deissmann, G.; Neumeier, S.; Brandt, F.; Modolo, G.; Bosbach, D. Evaluation of the Long-Term Behavior of Potential Plutonium Waste Forms in a Geological Repository. *MRS Online Proc. Libr.* **2014**, *1665*, 23−30.
(17) Icenhower, J. P.; Strachan, D. M.; Lindberg, M.; Rodriguez, E. A.; Steele, J. L. *Dissolution Kinetics of Titanate-Based Ceramic Waste Forms: Results from Single-Pass Flow Tests on Radiation Damaged Specimens*; Pacific Northwest National Laboratory: Richland, WA, 2003; Vol. *PNNL-14252*.
(18) Dacheux, N.; Du Fou de Kerdaniel, E.; Clavier, N.; Podor, R.; Aupiais, J.; Szenknect, S. Kinetics of Dissolution of Thorium and Uranium Doped Britholite Ceramics. *J. Nucl. Mater.* **2010**, *404* (1), 33−43.
(19) Finkeldei, S.; Brandt, F.; Rozov, K.; Bukaemskiy, A. A.; Neumeier, S.; Bosbach, D. Dissolution of ZrO2 Based Pyrochlores in the Acid pH Range: A Macroscopic and Electron Microscopy Study. *Appl. Geochem.* **2014**, *49*, 31−41.
(20) Corkhill, C. L.; Myllykylä, E.; Bailey, D. J.; Thornber, S. M.; Qi, J.; Maldonado, P.; Stennett, M. C.; Hamilton, A.; Hyatt, N. C. Contribution of Energetically Reactive Surface Features to the Dissolution of CeO2 and ThO2 Analogues for Spent Nuclear Fuel Microstructures. *ACS Appl. Mater. Interfaces* **2014**, *6* (15), 12279−12289.
(21) Horlait, D.; Claparede, L.; Tocino, F.; Clavier, N.; Ravaux, J.; Szenknect, S.; Podor, R.; Dacheux, N. Environmental SEM Monitoring of Ce 1− x Ln x O 2− x/2 mixed-oxide Microstructural Evolution during Dissolution. *J. Mater. Chem. A* **2014**, *2* (15), 5193−5203.
(22) Bosbach, D.; Charlet, L.; Bickmore, B.; Hochella, M. F. The dissolution of Hectorite: In-situ, Real-time Observations using Atomic Force Microscopy. *Am. Mineral.* **2000**, *85* (9), 1209−1216.
(23) Metz, V.; Raanan, H.; Pieper, H.; Bosbach, D.; Ganor, J. Towards the Establishment of a Reliable Proxy for the Reactive Surface Area of Smectite. *Geochim. Cosmochim. Acta* **2005**, *69* (10), 2581−2591.
(24) Ruiz-Agudo, E.; Putnis, C. V. Direct Observations of Mineral-fluid Reactions using Atomic Force Microscopy: the Specific Example of Calcite. *Mineral. Mag.* **2012**, *76* (1), 227−253.
(25) Putnis, A.; Junta-Rosso, J. L.; Hochella, M. F. Dissolution of Barite by a Chelating Ligand - an Atomic-Force Microscopy Study. *Geochim. Cosmochim. Acta* **1995**, *59* (22), 4623−4632.
(26) Luttge, A.; Arvidson, R. S.; Fischer, C. A Stochastic Treatment of Crystal Dissolution Kinetics. *Elements* **2013**, *9* (3), 183−188.
(27) Fischer, C.; Arvidson, R. S.; Luttge, A. How Predictable are Dissolution Rates of Crystalline Material? *Geochim. Cosmochim. Acta* **2012**, *98*, 177−185.
(28) Emmanuel, S.; Levenson, Y. Limestone Weathering Rates Accelerated by Micron-Scale Grain Detachment. *Geology* **2014**, *42* (9), 751−754.
(29) Levenson, Y.; Emmanuel, S. Pore-scale Heterogeneous Reaction Rates on a Dissolving Limestone Surface. *Geochim. Cosmochim. Acta* **2013**, *119* (0), 188−197.
(30) Godinho, J. R. A.; Piazolo, S.; Evins, L. Z. Effect of Surface Orientation on Dissolution Rates and Topography of CaF2. *Geochim. Cosmochim. Acta* **2012**, *86* (0), 392−403.
(31) Finkeldei, S.; Brandt, F.; Bukaemskiy, A.; Neumeier, S.; Modolo, G.; Bosbach, D. Synthesis and Dissolution Kinetics of Zirconia based Ceramics. *Prog. Nucl. Energy* **2014**, *72* (0), 130−133.
(32) Finkeldei, S. Pyrochlore as Nuclear Waste Form: Actinide Uptake and Chemical Stability. *PhD Thesis*, RWTH Aachen, Germany, 2014.
(33) Arvidson, R. S.; Fischer, C.; Sawyer, D. S.; Scott, G. D.; Natelson, D.; Lüttge, A. Lateral Resolution Enhancement of Vertical Scanning Interferometry by Sub-Pixel Sampling. *Microsc. Microanal.* **2014**, *20* (01), 90−98.
(34) Fischer, C.; Luttge, A. Converged Surface Roughness Parameters - A New Tool to Quantify Rock Surface Morphology and Reactivity Alteration. *Am. J. Sci.* **2007**, *307* (7), 955−973.
(35) Thomas, T. R. *Rough Surfaces*; Imperial College Press: London, 1999; p 278.
(36) Lasaga, A. C.; Luttge, A. Variation of Crystal Dissolution Rate Based on a Dissolution Stepwave Model. *Science* **2001**, *291* (5512), 2400−2404.
(37) Noiriel, C.; Gouze, P.; Bernard, D. Investigation of Porosity and Permeability Effects from Microstructure Changes during Limestone Dissolution. *Geophys. Res. Lett.* **2004**, *31*, 24.
(38) Daval, D.; Martinez, I.; Guigner, J.-M.; Hellmann, R.; Corvisier, J.; Findling, N.; Dominici, C.; Goffé, B.; Guyot, F. Mechanism of Wollastonite Carbonation Deduced from Micro-to Nanometer Length Scale Observations. *Am. Mineral.* **2009**, *94* (11−12), 1707−1726.

DOI: 10.1021/acsami.5b04281
ACS Appl. Mater. Interfaces 2015, 7, 17857−17865